The European Journal of Mineral Processing and Environmental Protection
Vol.4, No.3, 1303-0868, 2004, pp. 260-271

ejmp&ep

A digital imaging based approach to characterize arsenic minerals in colemanite ores

G. Bonifazi*, P. Massacci, S. Serranti

Dipartimento di Ingegneria Chimica, dei Materiali, delle Materie Prime e Metallurgia, Universita' degli Studi di Roma "La Sapienza", Via Eudossiana, 18, 00184 Rome, Italy

Received 2 February 2003; accepted 27 July 2004

ABSTRACT

The presence of considerable amount of arsenic in borate concentrate produces penalty in marketing and makes its removal necessary. In this perspective, an automated procedure based on structural and textural characterization of a colemanite ore, in order to evaluate the degree of liberation of the arsenic minerals, adopting image analysis techniques, is presented. Samples of a colemanite ($Ca_2B_6O_{11}•5H_2O$) concentrate coming from Turkey have been collected. It has been revealed the occurrence of colemanite in different sizes and shapes, most commonly in nodules (up to 50cm), sometimes with thin discontinuous layers of clay. The samples are affected by relevant concentration of two arsenic minerals, realgar (AsS) and orpiment (As_2S_3). Polished sections have been submitted to scanning electron microscopy (SEM) and optical microscopy in order to acquire suitable digital images. The arsenic minerals have been found either as disseminated crystals or in veinlets along colemanite fractures with a very thin size (up to 100μm). In order to characterise and quantify the complex and variable distribution of the As minerals, fully imaging based strategies have been set up and applied. The obtained results enabled to define suitable and reliable comminution strategies in order to liberate the arsenic minerals. The developed procedure can be successfully applied to other ores, constituted by mineral association characterised by complex textures.

Keywords: Colemanite; Boron; Degree of liberation; Image analysis; Arsenic removal

1. INTRODUCTION

Colemanite ($2CaO•3B_2O_3•5H_2O$) belongs to the family of borates and it is one of the few boron minerals of commercial importance, being used in a lot of industrial applications as: glass, metallurgy, cement, steel, textile, leather, cosmetics, soap and detergent, nuclear energy and agriculture (Industrial Minerals, 2002).

Despite the wide range of applications of boron minerals, their source of supply is very limited. One of the largest boron reserves in the world is located in the Mediterranean basin (in Turkey). The Turkish boron ores have high boron contents, but some of them are affected by considerable amount of arsenic minerals that contaminate the tailings coming from the chemical process treatment. In fact, for boric acid (H_3BO_3) extraction, the colemanite concentrate is leached by sulphuric acid (H_2SO_4) following the reaction:

$$2CaO•3B_2O_3•5H_2O+2H_2SO_4+6H_2O \rightarrow 2CaSO_4•2H_2O+6H_3BO_3 \quad (1)$$

The resulting waste, constituted by a boro-gypsum mud, entraps insoluble minerals.

In order to obtain a waste product contaminant-free, it could be profitable to leach the colemanite concentrates after reduction of the content of As minerals. In this perspective, a digital imaging based approach has been applied to a colemanite concentrate contaminated by the presence of arsenic minerals in order to characterise the particle texture and to evaluate their separability by flotation. In fact, the texture of an ore is of great interest in mineral processing as it affects particle behaviour in different mineral processing operation.

In this work, the degree of liberation of the exposed surface (DL_{ES}) of the mineral constituents has been calculated, in order to define:

- The size of the particles to obtain grains presenting the highest exposed surface of colemanite,
- The liberation modalities to evaluate the effect of comminution on the intergrowth minerals.
- The exposed topological assessment of colemanite (surface texture) has been also analysed.

* Corresponding author. E-mail: giuseppe.bonifazi@uniroma1.it

2. BORATE PRODUCTION AND DEPOSITS

There are over 200 boron-bearing minerals occurring worldwide, but only a few are commercially exploited (Table 1) and at very few locations. The four minerals comprised almost 90% of the borates used by industry worldwide are borax and kernite (sodium borates), colemanite (calcium borate) and ulexite (sodium-calcium borate) (Lyday, 2002). The main global supplier for borates is in Anatolia (Turkey) followed by North America and South America (Table 2). Russia and China also produce significant quantities of borates, but they export very little abroad.

Table 1
Main borate minerals of commercial importance (after O'Driscoll, 2001)

Mineral	Formula	B_2O_3 %
Na Borates		
Kernite	$Na_2B_4O_7 \cdot 4H_2O$	51.0
Tincal	$Na_2B_4O_7 \cdot 10H_2O$	36.5
Tincalconite	$Na_2B_4O_7 \cdot 5H_2O$	47.8
Ca Borates		
Colemanite	$Ca_2B_6O_{11} \cdot 5H_2O$	50.8
Datolite	$CaBSiO_4(OH)$	21.8
Inyoite	$Ca_2B_6O_{11} \cdot 13H_2O$	37.6
Priceite	$Ca_4B_{10}O_{19} \cdot 7H_2O$	49.8
Ca-Na Borates		
Probertite	$NaCaB_5O_9 \cdot 5H_2O$	49.6
Ulexite	$NaCaB_5O_9 \cdot 8H_2O$	43.0
Ca-Mg Borates		
Hydroboracite	$CaMgB_6O_8(OH)_6 \cdot 3H_2O$	50.5
Mg Borates		
Boracite	$Mg_6B_{14}O_{26}Cl_2$	62.2
Szaibelyite	$MgBO_2(OH)$	41.4

As shown in Fig. 1, borate deposits are located in continental tertiary areas of western Anatolia and American continent (Himalayan Mountains and Andes) (Floyd *et al.*, 1998). Borate deposits appear to have been formed by geothermal springs rising along fault zones related to volcanic activity associated with plate-tectonic subduction zones (Smith, 2002). Moreover, the formation of a large borate deposit requires an arid climate in presence of a closed basin with a depth suitable for salts accumulation.

Concerning Turkey, the boron deposits are located in four districts in the western part of the country, i.e. in Eskişehir-Kirka (tincal), in Kütahya-Emet and Bursa-Kestelek (colemanite) and in Balikesir-Bigadiç (colemanite and ulexite). They were formed in a lacustrine environment during calc-alkaline volcanic activity in the Neogene (Palmer and Helvaci, 1997; Helvaci and Alonso, 2000). The borates of all districts are generally enclosed within limestones and clays and are interbedded with layers of volcanic ash, limestone, marl and clays. The boron probably derived from leaching of the surrounding rocks by geothermal activity associated with local volcanism. The borates were formed after evaporation of waters flowing into shallow playa lakes (Helvaci, 1995).

Table 2
World production and reserves of borates, by country (after Lyday, 2004). Data in thousand metric tons of boric oxide (B_2O_3)

Country	Production – all forms		Reserves
	2002	2003[e]	
Argentina	510	170	2,000
Bolivia	35	33	NA
Chile	330	430	NA
China	145	140	25,000
Iran	4	4	1,000
Peru	9	9	4,000
Russia	1,000	1,000	40,000
Turkey	1,500	1,500	60,000
USA	1,050	1,060	40,000
Total	4,580	4,350	170,000

[e] Estimated. NA: Not Available

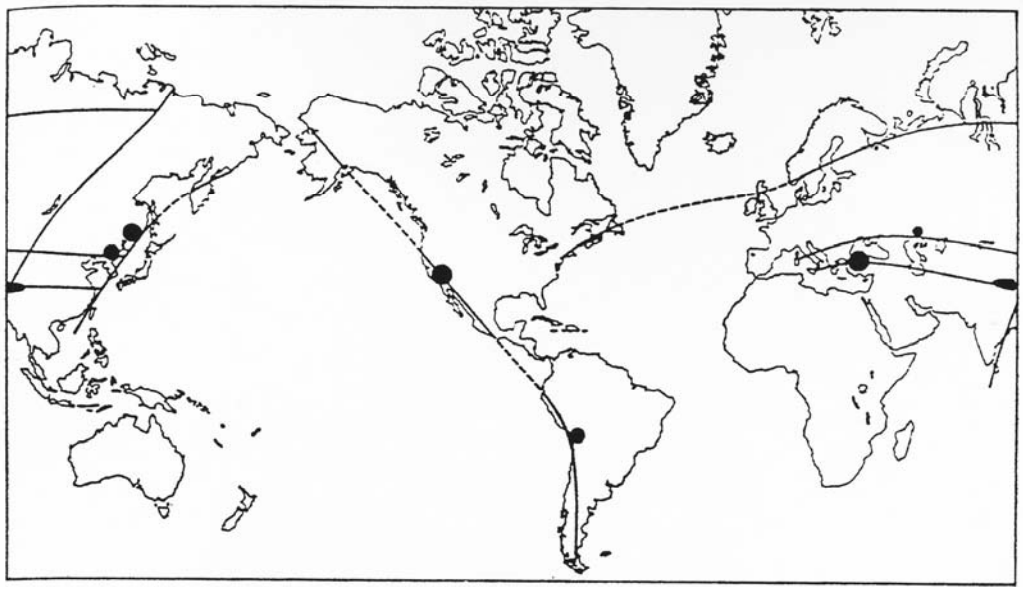

Figure 1. Location of borate reserves in the world and suggested uplifted rift-subduction zone correlation (after Garrett, 1998)

3. MATERIALS AND METHODS

Representative samples of a colemanite concentrate coming from Turkey have been collected from the product fed to a boric-acid plant located in Larderello, Tuscany, Italy.

Some samples have been prepared as polished sections for study by optical and SEM.

In order to estimate the degree of liberation of the mineral constituents, the following strategy, based on image analysis techniques, has been adopted:

- Structural and textural characterisation of the colemanite concentrate and the related products coming from mineral processing;
- Comminution of the colemanite ores;
- Acquisition of digital images by SEM from the comminution products;
- Digital images processing for acquisition of particle geometrical features and topological assessment of the different mineral constituents;
- Data interpretation.

4. SAMPLE DESCRIPTION

In hand specimens colemanite occurs in well-formed coarse sized prismatic crystals with colour ranging from grey, grey white, yellowish white and white. The crystals commonly form nodules (up to 50 cm), showing radiating structures. Colemanite crystals are usually separated by thin discontinuous layers of clay. Two arsenic minerals, realgar (AsS) and orpiment (As_2S_3), are well recognized by their typical colour, red and yellow, respectively. They are disseminated in colemanite lumps or form veinlets along colemanite discontinuities.

From microscopic observations, it appears that realgar occurs either as disseminated subhedral crystals of variable size inside the colemanite lumps or in veinlets with usually a thin size (up to 100μm) (Figs. 2, 3, 4 and 5).

The crystal size is, on average, about hundred microns but can reach up to some millimetres. Orpiment usually occurs as disseminated fine grains in contact and into a clay matrix filling colemanite fractures (Figs. 3 and 6) or separating colemanite crystals. The small orpiment crystals have an acicular shape of 20÷30μm in length and about 5μm in width. Another accessory mineral is celestine ($SrSO_4$) occurring associated with colemanite. Celestine occurs as subhedral prismatic crystals disseminated in colemanite lumps (Fig. 5) with a size ranging from few microns up to 100μm.

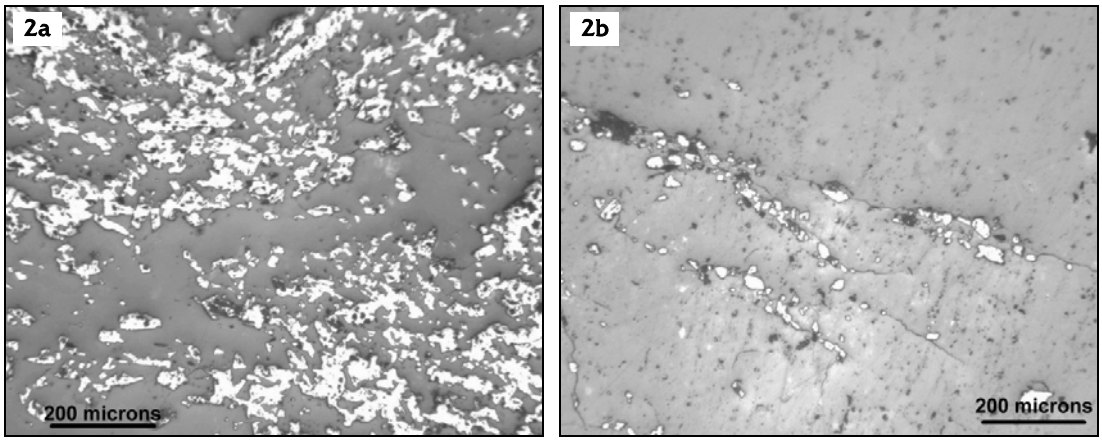

Figure 2. Colemanite ($Ca_2B_6O_{11}\cdot 5H_2O$) showing dissemination of realgar (AsS) (optical microscopy, reflected light, 100x). Such dissemination usually occurs both as dispersion of fine particles in colemanite and small plagues characterised by complex boundaries (2a) and as fine veinlets along colemanite discontinuities (2b)

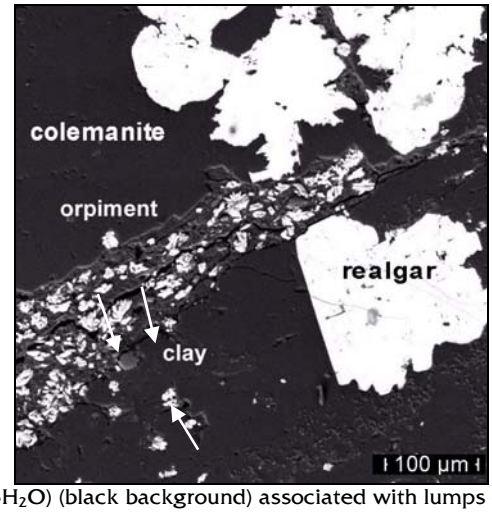

Figure 3. Colemanite ($Ca_2B_6O_{11}\cdot 5H_2O$) (black background) associated with lumps of realgar (AsS) (white) and finely disseminated particles of orpiment (As_2S_3) (white) in a clay lump (grey) filler of a fracture (SEM - BSE)

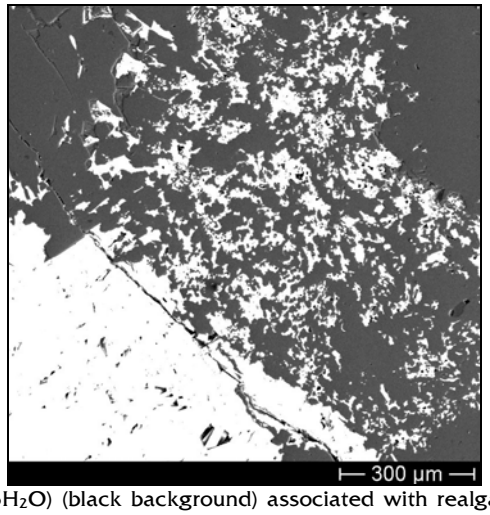

Figure 4. Colemanite ($Ca_2B_6O_{11}\cdot 5H_2O$) (black background) associated with realgar (AsS) (white) occurring as fine disseminated particles and as a big subhedral crystal (SEM - BSE)

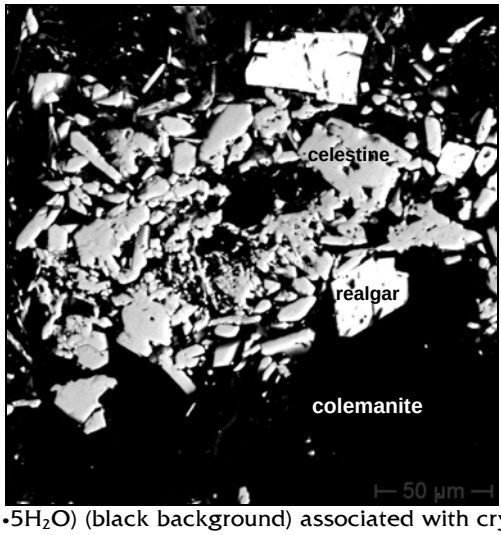

Figure 5. Colemanite ($Ca_2B_6O_{11}•5H_2O$) (black background) associated with crystals of celestine ($SrSO_4$) (light grey) and realgar (AsS) (white) (SEM - BSE)

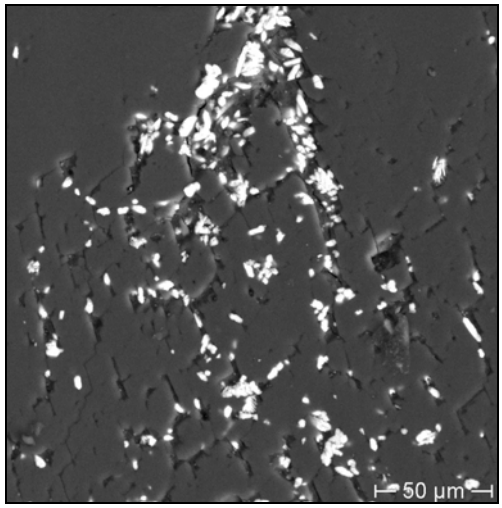

Figure 6. Colemanite ($Ca_2B_6O_{11}•5H_2O$) (black background) with finely disseminated particles of orpiment (As_2S_3) (white) in a clay matrix (grey) (SEM - BSE)

5. COMMINUTION AND ACQUISITION OF DIGITAL IMAGES

The investigated samples result from a combined comminution-wet screening process carried out at laboratory scale (Massacci *et al.*, 2003). In Table 3 the size distribution of the analysed samples and the corresponding As contents are given. The analyses show the increasing trend of As content as the particle size decreases.

Table 3
Size distribution and As content of the colemanite concentrate after comminution

Particle Size µm	Weight %	As ppm
+250	0.94	800
-250 +125	15.83	675
-125 +75	23.73	923
-75 +38	23.05	1220
-38	36.45	3850
Feed	100.00	2050

Polished sections, enclosing particles of the different particle sizes, have been prepared for SEM analysis. The samples are characterized by free colemanite particles and mixed particles composed of colemanite and other mineral species in different proportions.

Twenty images were randomly acquired from a sample of each size-class using a HITACHI 2500 SEM in BSE modality. The images have been acquired with the dynamic of 8 bit/pixel and a resolution of 800 x 1000 pixels. In order to acquire a suitable number of particles from each image (about 5 particles), different magnifications have been selected, according to the different size range, as reported in Table 4. An example of the acquired digital images for each size-class is reported in Fig. 7.

Table 4
Magnifications adopted for image acquisition by SEM

Particle size µm	Magnification
- 250 + 125	300x
- 125 + 75	400x
- 75 + 38	800x
- 38	1500x

6. DIGITAL IMAGE PROCESSING

The imaging procedure has been developed using Image-Pro Plus™ software by Media Cybernetics and adopting the Auto-Pro™ macro language for original and automatic routines running.

Eighty acquired digital images have been processed in order to obtain information on the recurrence of colemanite and other mineral species present in each particle. The different mineral species have been recognized from the digital images on the basis of their different grey level tone, related to the corresponding chemical composition. In fact, it is well known that the grey level tone characterising a mineral observed by SEM, in BSE modality strongly depends on the atomic number of the chemical elements constituting the structure. In particular, the level of grey tone increases, from darker to brighter ones, passing from minerals containing "light" to those containing "heavy" elements. In fact, as it can be noticed in Fig. 7, colemanite appears to be darker than arsenic minerals and celestine.

The following procedure has been adopted:

- The particles are segmented from the "dark" background on the basis of their grey level characteristics. Three grey-level classes (Fig. 8) are considered: dark background with a grey-level ranging from 0 to 90, colemanite with a grey-level ranging from 91 to 210 and the other mineral species (celestine, realgar and orpiment) showing a grey-level ranging from 211 to 255,
- The segmentation is obtained by setting the range of the grey-levels that correspond to the mineral species to identify,
- The identified particles are counted and the measurements of some morphological parameters, characterising the different mineral species are performed. The counting is obtained ignoring particles not completely recognizable, lying at the borders of the image, as they can skew the results.

7. COMPUTATION OF THE DEGREE OF LIBERATION OF THE EXPOSED SURFACES

From the digital images acquired for the four size classes obtained after comminution, the degree of liberation of the exposed surfaces (D_{LES}) has been calculated.

First, the following area parameters are extracted (Fig. 9): Area of each particle (Ap), area of colemanite (grey) in each particle (Ac), area of other minerals (white) in each particle (Ao).

The D_{LES} of colemanite, for each size-class, was then computed according to the formula:

$$D_{LES} = \frac{\sum A_f}{\sum A_t} \tag{2}$$

where: ΣAf is the sum of area of free colemanite particles and ΣAt is the sum of area of total colemanite (free + mixed particles). The D_{LES} of the other mineral species (celestine, realgar and orpiment) was computed adopting the same criterion. The results obtained after D_{LES} computations are reported in Fig. 10.

The D_{LES} of colemanite results quite high for all the obtained size class distribution, presenting on average a value over 0.976 and reaching the value of 0.999, practically totally free mineral, for particles below 38μm. On the contrary, the D_{LES} for the other mineral species is equal to zero for the coarser particles, until about 80μm. Below such a size, it suddenly increases, reaching a value of about 0.60 for the particulate products under 38μm. Together with a very high degree of liberation of colemanite at the finest size class (e.g. Fig. 7d), it can be detected as in coarse fractions colemanite often results contaminated by the presence of small amount of polluting minerals (e.g. Figs. 7a and 7b), as realgar, usually finely disseminated.

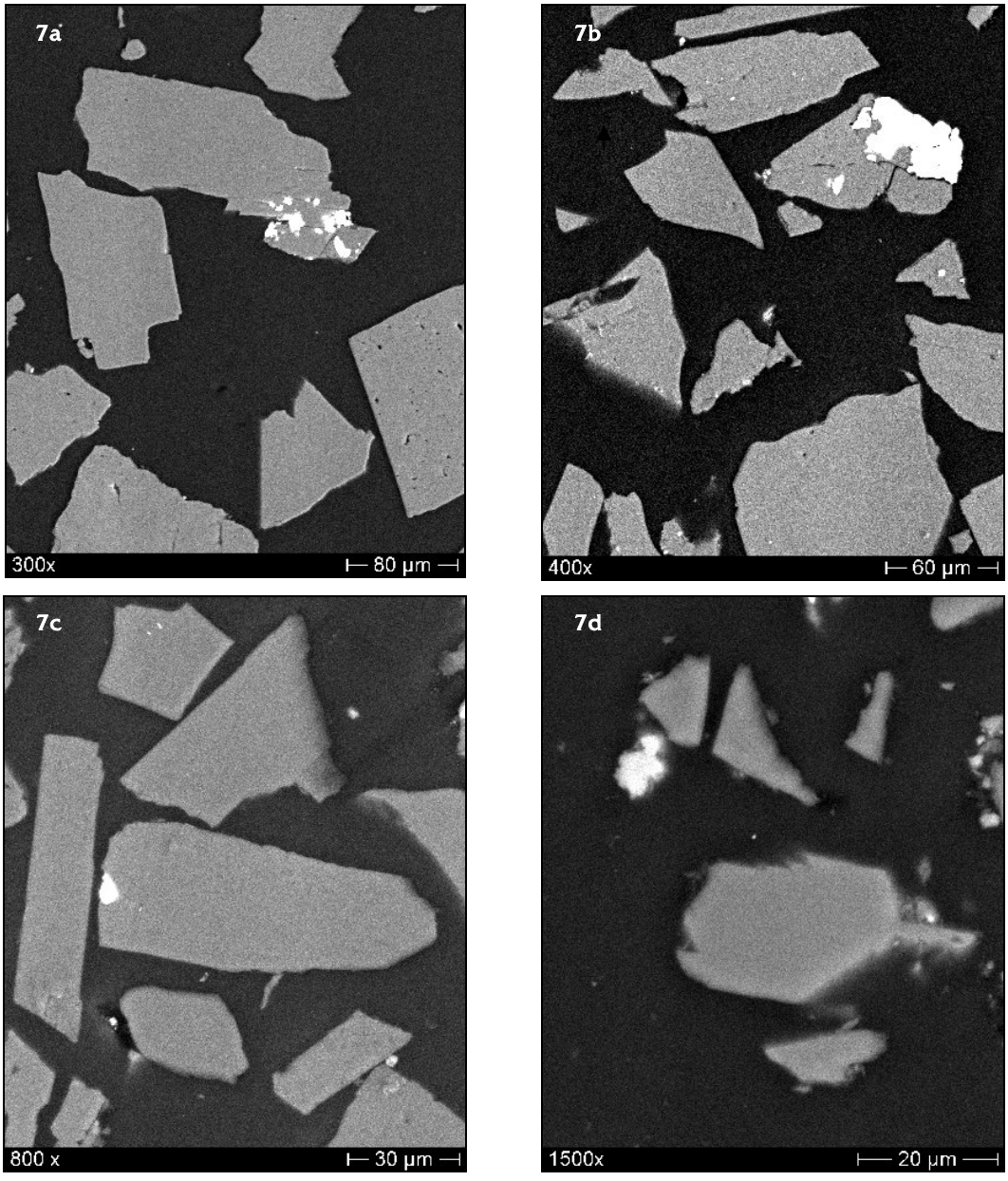

Figure 7. Digital images (SEM-BSE) representative of the four size-classes obtained by comminution of the colemanite acquired under different magnifications. 7a, 7b, 7c and 7d are respectively referred to the particle sizes: -250 +125μm, -125 +75μm, -75 +38μm and -38μm

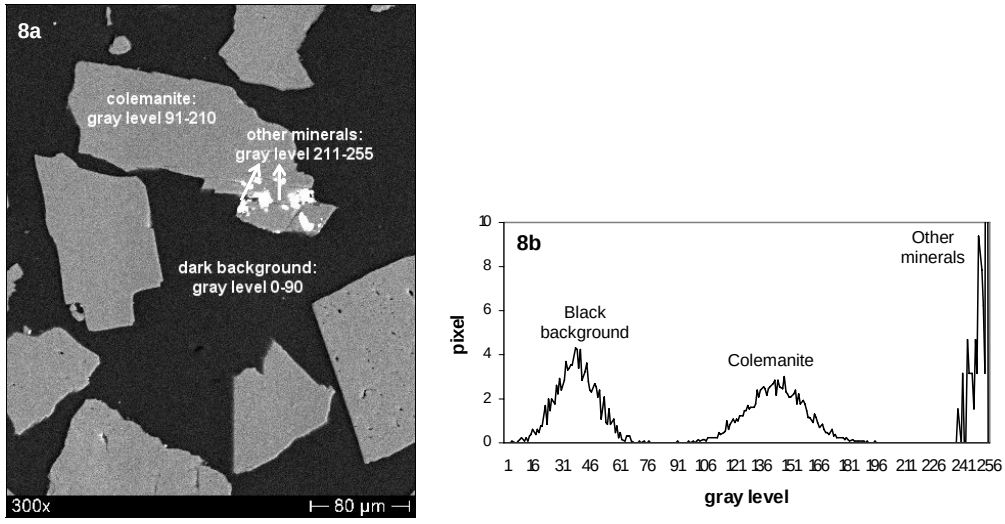

Figure 8. Digital image (SEM-BSE) (8a) of particles coming from comminution of the colemanite concentrate. Three well separated grey-level histograms correspond to different mineral species (8b)

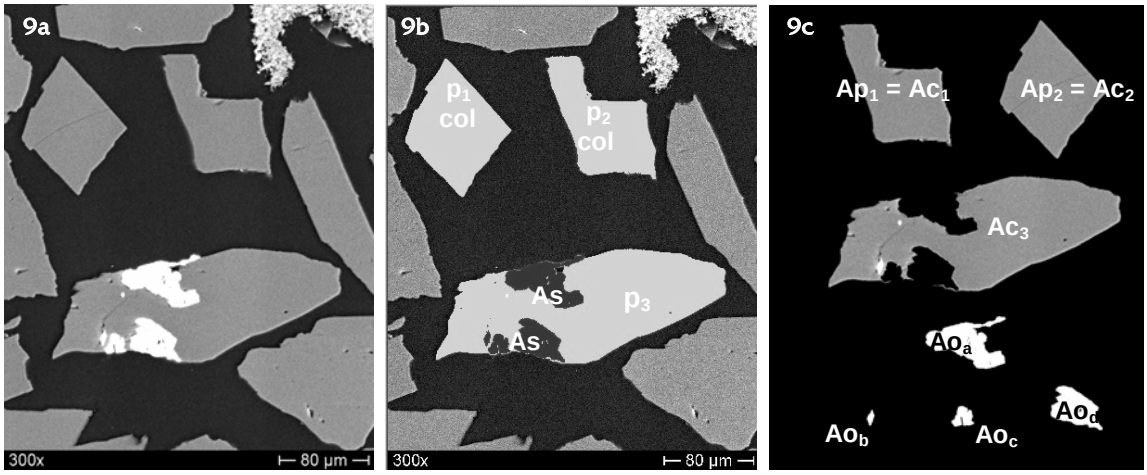

Figure 9. Example of counting of free and mixed particles. 9a: source digital image (SEM-BSE). 9b: the same image after segmentation. For the particles (p_1, p_2 and p_3) the projected area has been evaluated. For each one the area was evaluated. 9c: area computation. For particle 1 (p_1) the computed area (Ap_1) corresponds to the area of colemanite mineral (Ac_1), being a free particle; the same happens for particle 2 (p_2). Concerning the locked particle 3 (p_3), the computed area (Ap_3) is given by the sum of the area of colemanite mineral (Ac_3) and the area of other minerals (Ao_3), according to the following formula: $Ap_3 = Ac_3+Ao_3$. The latter area is obtained by the sum of the four identified white particles: $Ao_3 = Ao_a+Ao_b+A_oc+Ao_d$

8. COMPUTATION OF THE SURFACE TOPOLOGICAL ASSESSMENT OF THE DIFFERENT MINERAL SPECIES

It is important to know not only the amount of the species of interest in relation to the associated gangue in each particle, but also their distribution, that is the topological assessment. Such parameter was computed for the different mineral species starting from the relative position of the centre of gravity of each identified domain belonging to every recognized mineral. Handling of this information together with the morphological and the morphometrical attributes of the species allowed classifying each particle not only on the base of the degree of liberation of the exposed surfaces (D_{LES}), but also in terms of textural characteristics. Following this way each class of particles can be defined in terms of its further processing behaviour. Leaching and/or flotation process are, in fact, strongly influenced by the distribution of the constituent minerals inside each particle.

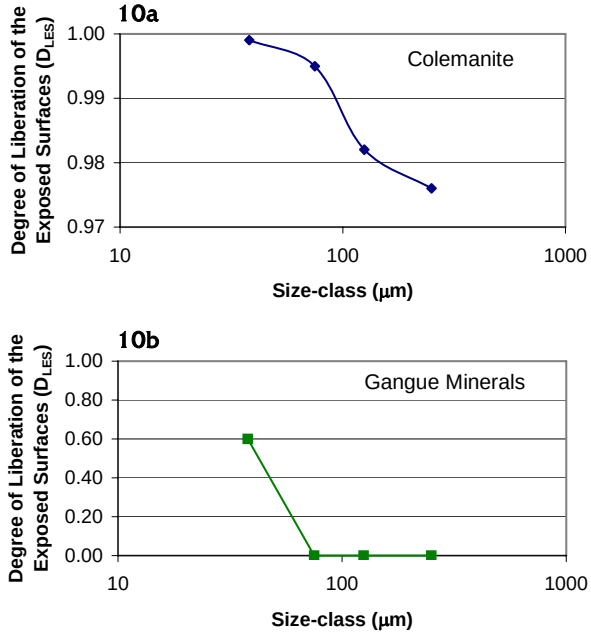

Figure 10. Degree of liberation of the exposed surfaces (D_{LES}) for the different size-class samples of colemanite examined in the study (10a) and other minerals (realgar, orpiment and celestine considered as a "unique gangue") (10b). It is clearly detectable as colemanite presents, differently from the "gangue", a very high D_{LES} in all the samples. Such a parameter starts to reach significant values for the "gangue" only for samples with a size class distribution below 38μm

Assuming CG_{ij} (x_j, y_j) as the coordinates of the j-th centre of gravity of the i-th mineral species (i.e. realgar), and extracting, by imaging, for each ij domain the numerical information related to their size and shape characteristics, two sets of data structure can be thus defined, that is:

- A topological plot, modelling for each particle the relative distribution of the mineral species inside the particle itself (Fig. 11);
- A matrix able to describe the overall textural attributes of the mineral species (2D distribution and geometrical characteristics) (Fig. 12) inside the whole set of particles constituting the material to process.

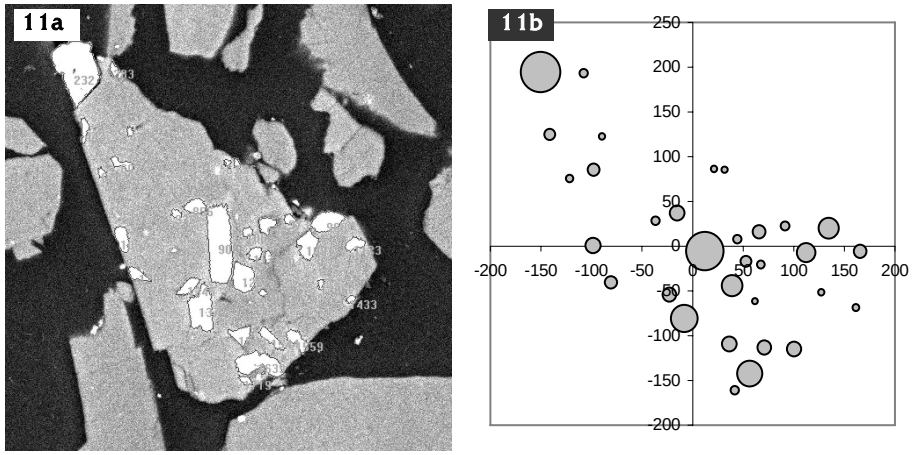

Figure 11. Example of topological plot for a locked colemanite particle. 11a: digital processed image showing domain identification, counting, morphological attribute evaluation for the different inclusions of "other mineral species"inside a colemanite particle. 11b: plot of the position of each single inclusion of "other mineral species" in respect to the centre of gravity of the colemanite particle (identified by the coordinates x= 0 and y = 0). The area of the circles, representing each inclusion, is proportional to that of the corresponding particles

An example of topological plot is reported in Fig. 11. The image, representing the locked particle of colemanite (Fig. 11a), has been processed and the morphological and morphometrical parameters of each single inclusion have been measured together with their xy-coordinates. The plot of Fig. 11b represents location of each inclusion of "other mineral species" in respect with the centre of gravity of the locked colemanite particle; in addition, at each point it is associated a circle having a diameter proportional to the size of the particle areas. Adopting the same procedure, starting from the centre of gravity of each identified domain, other morphometrical parameters can be numerically defined and plotted, stressing this way information usually difficult to quantify.

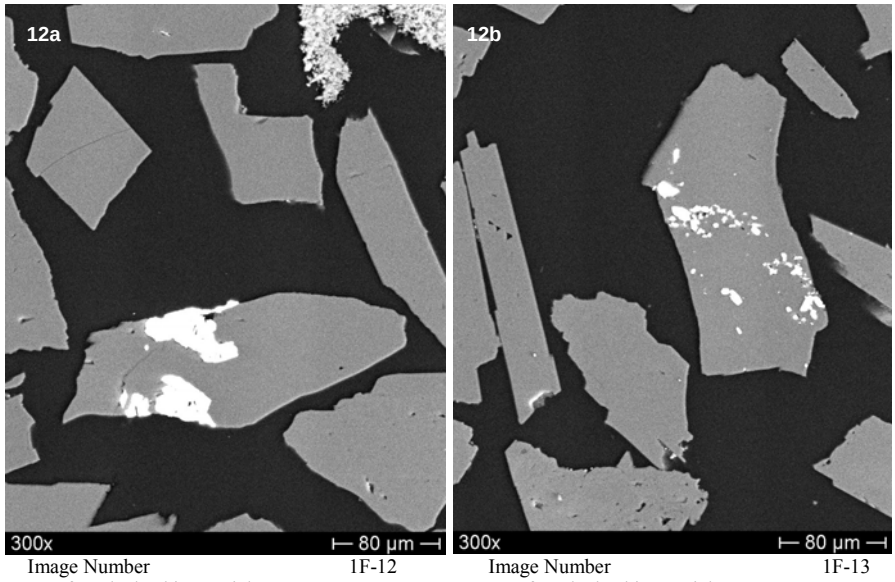

Image Number	1F-12	Image Number	1F-13
N° of Locked White Particles	4	N° of Locked White Particles	33
Average Area of Particles (μm^2)	748	Average Area of Particles (μm^2)	32

Figure 12. Example of locked particles characterised by different textural attributes. 12a: colemanite mineral is assembled with few and big white particles of "other mineral species"; 12b: the colemanite is linked with several and small white particles of "other mineral species". Textural differences are quantified by the measured parameters (number of particles and average area) reported for each image

Interesting results have been obtained considering the "aspect" parameter of each identified domain. Such a parameter is representative of the ratio between the major axis and the minor axis of an ellipse characterised by the same surface of the domain. The aspect is always ≥ 1.

Comparing the aspect of the free and locked colemanite particles, belonging to the different size class distribution, it appears that the locked colemanite particles (as recognized for each class) tend to roundness more than the free colemanite particles (Fig. 13). In addition, the particle elongation increases as the size class for both free and locked colemanite decreases (Fig. 14).

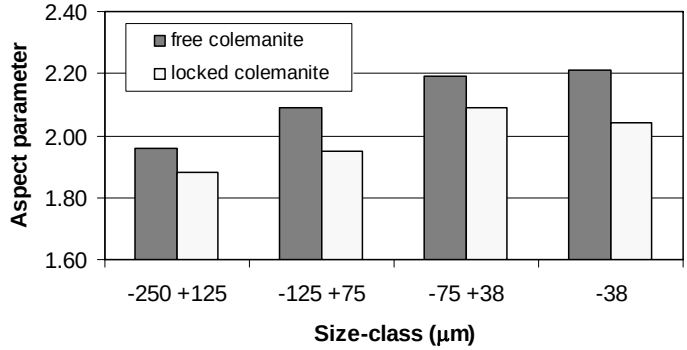

Figure 13. Aspect parameter plotted after digital image processing applied to free and locked colemanite particles for the four investigated size-classes. "Aspect" parameter is representative of the particle elongation

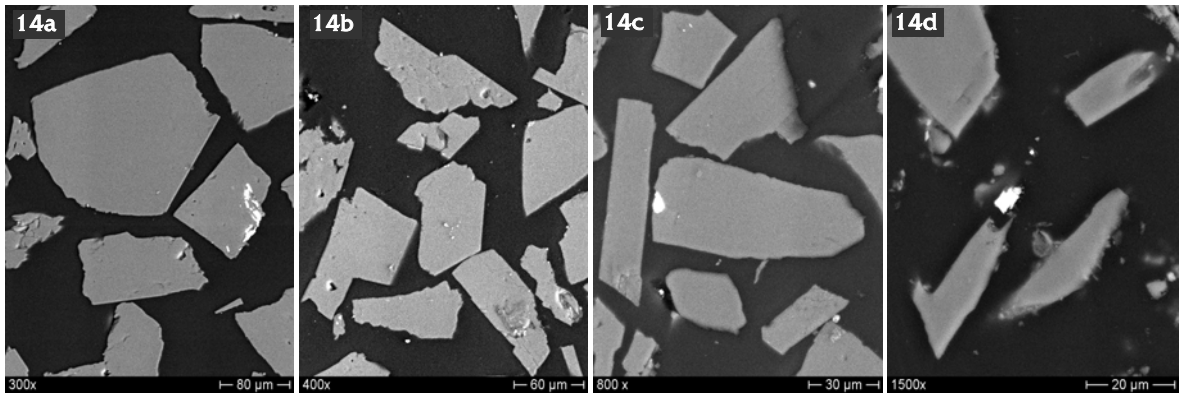

Figure 14. The image sequence shows the identified trend concerning the colemanite particle aspect. Particle elongation increases as the size-class decreases. 14a: -250 +125µm, 14b: -125 +75µm, 14c: -75 +38µm and 14d: -38µm

9. CONCLUSIONS

The implemented strategy, based on imaging, has been addressed to quantify the degree of liberation of each mineral species on the exposed surface of each particle. Such a procedure results quite powerful when mineral processing strategies, specifically addressed to utilise mineral surface properties, as flotation, have to be set up. On these bases, textural numerical characterisation of the ore and of the particles, resulting from comminution, allow properly defining beneficiation (i.e. combined comminution-flotation processes) and control strategies (i.e. topological imaging based mineral species assessment in the particle concentrate) to maximize colemanite recovery.

The results achieved in this study clearly demonstrated as a combined used of classical SEM analyses and innovative imaging based procedures play a fundamental role in the selection of beneficiation flow-sheet related to ore mineral characterised by a complex texture. Such an approach, in fact, allow to numerically quantify not only the quantity of the species of interest but also its 2D spatial distribution (according to the selected thin or polished section sample sets) inside the ore and/or the products (grains), resulting from the different stage of processing. The procedure was successfully applied to define an optimal flotation circuit, based on two stages grinding and flotation of As bearing minerals (Massacci *et al.*, 2003). Further studies are addressed to realise a 2D topological models able to describe the ore and /or the particle not only with reference to the species of interest but taking into account the contemporary presence, in the examined sample set, of the different mineral species.

ACKNOWLEDGEMENTS

Thanks are given to Mr. Carmine Panzironi for helping in SEM analyses and to Mr. Massimo Delfini for sample preparation, both carried out at the Department of Chemical, Materials, Raw Materials and Metallurgy, Faculty of Engineering of the University "La Sapienza" of Rome. Special thanks have to be addressed to "Società Chimica Larderello S.p.A." for its support to this investigation.

REFERENCES

Floyd, P.A., Helvaci, C., Mittwede, S.K., Geochemical discrimination of volcanic rocks associated with borate deposits: an exploration tool?. Journal of Geochemical Exploration, 1998, 60, 185-205.

Garrett, D.E., Borates, Handbook of Deposits, Processing, Properties and Use, 1998, Academic Press Ed., San Diego, 483 p.

Helvaci, C., Stratigraphy, mineralogy and genesis of the Bigadic borate deposits, western Turkey. Econ. Geol., 1995, **90,** 1237-1260.

Helvaci, C. and Alonso, R.N., Borate deposits of Turkey and Argentina; A summary and geological comparison. Turkish Journal of Earth Sciences, 2000, **9**, 1-27.

Industrial Minerals, Boron Minerals. February 2002.

Lyday, P.A., Boron. U.S. Geological Survey Minerals Yearbook, 2002.

Lyday, P.A., Boron. U.S. Geological Survey, Mineral Commodity Summaries, January 2004, pp. 36-37.

Massacci, P., Serranti, S., Ghiani, M., Peretti, R., Zucca, A., Manni, A., Reduction of the As content in colemanite concentrates. Proceedings XXII International Mineral Processing Congress, 29 September – 3 October 2003, Cape Town, South Africa, 543-551.

O'Driscoll, M., Borates. The Turk of the town. Industrial Minerals, March 2001, pp. 30-45.

Palmer, M.R. and Helvaci, C., The boron isotope geochemistry of the neogene borate deposits of western Turkey. Geochimica et Cosmochimica Acta, 1997, **61**, 3161-3169.

Smith, R.A., Basic geology and chemistry of borate. American Ceramic Society Bulletin, 2002, **81**, 8.